MITSUBISHI ELECTRIC RESEARCH LABORATORIES
http://www.merl.com

Near-field enhancement of thermoradiative devices

Lin, C.; Wang, B.; Teo, K.H.; Zhang, Z.

TR2017-153 October 2017

Abstract

Thermoradiative (TR) device has recently been proposed for noncontact direct photon-electricity energy conversion. We investigate how the near-field effect can boost the performance of a TR device. For a near-field TR device, a heat sink is placed close to the TR cell, with the separation being small compared to the characteristic photon wavelength. It is demonstrated that the TR device, like the thermophotovoltaic (TPV) device, can be formulated using the transmissivity and the generalized Planck distribution. We quantitatively show that -function transmissivity is a very good approximation (capturing up to 90% of total radiative energy transfer) when the radiative energy transfer is governed by resonances. Three practical types of heat sink are considered, a metallic material described by the Drude model, a polar dielectric material described by the Lorentz oscillator model, and a semiconductor material that is identical to the TR cell. The blackbody heat sink serves as the far-field reference. By properly choosing the resonant frequencies supported by the heat sink, we show the heat sink made of a Drude or Lorentz material can enhance the output power by about 60 and 20 times respectively, as compared to the blackbody reference. Even with a heat sink made of the same material as the TR-cell, which does not support any resonant modes, the output power can be enhanced by about 10 times. The mechanisms can be elucidated from the impedance matching condition derived from coupled-mode theory.

Journal of Applied Physics

This work may not be copied or reproduced in whole or in part for any commercial purpose. Permission to copy in whole or in part without payment of fee is granted for nonprofit educational and research purposes provided that all such whole or partial copies include the following: a notice that such copying is by permission of Mitsubishi Electric Research Laboratories, Inc.; an acknowledgment of the authors and individual contributions to the work; and all applicable portions of the copyright notice. Copying, reproduction, or republishing for any other purpose shall require a license with payment of fee to Mitsubishi Electric Research Laboratories, Inc. All rights reserved.

Copyright © Mitsubishi Electric Research Laboratories, Inc., 2017
201 Broadway, Cambridge, Massachusetts 02139

Near-field enhancement of thermoradiative devices

Chungwei Lin, Bingnan Wang, Koon Hoo Teo
Mitsubishi Electric Research Laboratories, 201 Broadway, Cambridge, MA 02139, USA

Zhuomin Zhang
George W. Woodruff School of Mechanical Engineering,
Georgia Institute of Technology, Atlanta, GA 30332, USA
(Dated: September 20, 2017)

Thermoradiative (TR) device has recently been proposed for noncontact direct photon-electricity energy conversion. We investigate how the near-field effect can boost the performance of a TR device. For a near-field TR device, a heat sink is placed close to the TR cell, with the separation being small compared to the characteristic photon wavelength. It is demonstrated that the TR device, like the thermophotovoltaic (TPV) device, can be formulated using the transmissivity and the generalized Planck distribution. We quantitatively show that δ-function transmissivity is a very good approximation (capturing up to 90% of total radiative energy transfer) when the radiative energy transfer is governed by resonances. Three practical types of heat sink are considered, a metallic material described by the Drude model, a polar dielectric material described by the Lorentz oscillator model, and a semiconductor material that is identical to the TR cell. The blackbody heat sink serves as the far-field reference. By properly choosing the resonant frequencies supported by the heat sink, we show the heat sink made of a Drude or Lorentz material can enhance the output power by about 60 and 20 times respectively, as compared to the blackbody reference. Even with a heat sink made of the same material as the TR-cell, which does not support any resonant modes, the output power can be enhanced by about 10 times. The mechanisms can be elucidated from the impedance matching condition derived from coupled-mode theory.

PACS numbers:

I. INTRODUCTION

Thermoradiative (TR) devices [1–4], like photovoltaic (PV) devices [5, 6], are electric power generators that use the radiative energy transfer between reservoirs maintained at different temperatures. Unlike the PV devices where PV cells are kept at a lower temperature to generate electric current, in TR devices the TR cells that generate the electric power are kept at a higher temperature. The principle of both PV and TR cells is illustrated in Fig. 1. For a working PV cell at a temperature T_{cell}, a heat source is maintained at a higher temperature $T_s > T_{cell}$ [Fig. 1(b)]. Consequently, the absorbed photon flux is greater than the emitted, leading to an electron-hole (e-h) population larger than its equilibrium value at T_{cell}. The PV cell attempts to recover its equilibrium e-h population via any e-h recombination channels, including removing electrons from the conduction band through an external load to fill the valence band, which is the electric current one can use. For a working TR cell at a temperature T_{cell}, a heat sink is maintained at a lower temperature $T_s < T_{cell}$ [Fig. 1(c)]. Consequently, the absorbed photon flux is smaller than the emitted, leading to an e-h population smaller than its equilibrium value at T_{cell}. The TR cell attempts to recover its equilibrium e-h population via any e-h *generation* channels, including removing electrons from the valence band through an external load to fill the conduction band, which is again the electric current one can use. Other than the opposite current direction, PV and TR cells are equivalent from the microscopic point of view.

As the TR and PV devices share the same physical origin, approaches that enhance the PV performance also enhance the TR performance. Thermophotovoltaic (TPV) is a promising approach to enhance the PV performance. A basic TPV system consists of an emitter and a PV cell [7–12], with the emitter placed between the heat source and the PV cell and kept at a high temperature by a heat source. The main role of the emitter is to reshape the photon emission spectrum to better fit the bandgap of the PV cell. For the near-field based TPV system [13–19], the separation between the emitter and the PV cell is much shorter than the characteristic wavelength of the emitted photons, and the resulting radiative energy transfer can be up to 10^4 times greater than the blackbody limit [20–23]. The physics can be understood in the framework of coupled-mode theory (CMT) [24–30], where the radiative energy transfer between different reservoirs originates from their coupling to common resonant modes [31]. According to CMT, the strong enhancement in TPV system stems from the surface resonances supported by the emitter/vacuum interface.

CMT analysis also provides "impedance matching" conditions for the maximum radiative energy transfer: if both PV/vacuum and emitter/vacuum interfaces by themselves support their respective surface resonances, the radiative energy transfer is maximized when the complex resonant energies are identical (including real and imaginary parts); if there is only one resonant mode, the radiative energy transfer is maximized when the resonant mode decays to the PV cell and to the emitter at the same rate [27, 30, 32].

The near-field TPV concept can be applied to TR devices [4], where a heat sink is placed close to the high-temperature TR cell. The role of the heat sink is similar to the emitter in the TPV system – it reshapes the photon radiation spectrum to facilitate the radiative energy transfer from the TR cell to the heat sink. Following Refs. [3, 30], we show that the TR devices can also be completely described by the transmissivity (between the TR cell and the heat sink) and the generalized Planck distributions [33–35]. As the generalized Planck distribution is obtained from thermodynamics, the transmissivity, which is material and geometry specific but is independent of thermodynamic variables, completely determines the TR performance. We consider three types of heat sink materials – a metal whose dielectric function is described by the Drude model [36, 37], a Lorentz material described by the Lorentz oscillator model [4, 38, 39], and a heat sink with the same material as the TR cell. The blackbody heat sink serves as the reference. We only consider the planar structure, and the transmissivity is computed using the dyadic green function [40, 41] and the fluctuation-dissipation relation between the thermal current and temperature [42]. The rest of the paper is organized as follows. In section II, we provide a general and unified picture for both PV and TR devices. We show that the load output power and the efficiency can be expressed in terms of transmissivity and the generalized Planck distribution. We also quantitatively show that the δ-function transmissivity is a good approximation for the general near-field configuration. In section III we show our simulations for three types of heat sinks. The results are discussed and understood from the impedance matching condition derived from CMT. In particular, we show how the loss can sometimes enhance the TR performance, which has been demonstrated in PV devices [19]. A brief conclusion is given in Section IV.

II. GENERAL FORMALISM

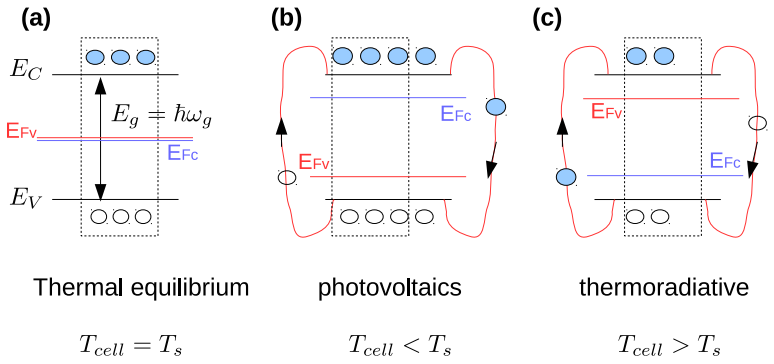

FIG. 1: Illustration on how photovoltaic and thermoradiative cells work, emphasizing their chemical nature. Here, T_{cell} is the temperature of the PV or TR cell, T_s is the temperature of the thermal reservoir (not shown), E_C and E_V represent the edges of the conduction band and valance band, respectively, and filled and hollow circles correspondingly denote electrons and holes. The dashed boxes represent equilibrium e-h population at T_{cell}. Blue and red lines indicate the electron and hole quasi-Fermi energies E_{Fc} and E_{Fv}, characterizing the electron and hole concentrations respectively. The photon chemical potential is given as $\mu = E_{Fc} - E_{Fv}$. (a) When the cell is in thermal equilibrium with the thermal reservoir, the emitted photon flux equals to the absorbed photon flux. The rate determines the equilibrium e-h population in the cell at T_{cell}. In this case, $E_{Fc} = E_{Fv}$ and $\mu = 0$. (b) For a PV cell, as the thermal reservoir is at a higher temperature, the absorbed photon flux (that creates e-h pairs) is greater than the emitted photon flux (that annihilates e-h pairs), leading to an e-h population greater than the equilibrium value, i.e. $E_{Fc} > E_{Fv}$ and $\mu > 0$. The PV cell tends to transfer electrons from the conduction band through an external load to fill the holes in the valence band. (c) For a TR cell, the emitted photon flux is greater than the absorbed, leading to an e-h population smaller than its equilibrium value, i.e. $E_{Fc} < E_{Fv}$ and $\mu < 0$. To recover its equilibrium population, the TR cell tends to transfer electrons from the valence band through an external load to the conduction band.

A. The formalism

To make the presentation self-contained, we recapitulate the radiative energy transfer using the transmissivity and the generalized Planck distribution [3, 30]. Given the transmissivity between the cell and a thermal reservoir (either a heat source or a heat sink) $\varepsilon_{c,s}(\omega)$, for the PV or TR cell, the absorbed photon flux minus the emitted is given by

$$\dot{N}(T_{cell}, \Delta\mu; T_s) = \int_{\omega_g}^{\infty} \frac{d\omega}{2\pi} \varepsilon_{c,s}(\omega) \left[\Theta(\omega; T_s, 0) - \Theta(\omega; T_{cell}, \Delta\mu)\right], \tag{1}$$

where the thermal reservoir is fixed at $T = T_s$, $\mu = 0$ whereas the cell is at $T = T_{cell}$, $\mu = \Delta\mu$. $\Theta(\omega; T, \mu) = [\exp[(\hbar\omega - \mu)/T] - 1]^{-1}$ is the generalized Planck distribution [33–35], with μ the photon chemical potential [43]. The photon chemical potential is related to the difference of quasi-Fermi energies, as illustrated in Fig. 1. We take Boltzmann constant $k_B \equiv 1$, so the temperature T is understood as $k_B T$ with the dimension of energy. The lower bound of the integral $\hbar\omega_g \equiv E_g$ is the bandgap: photons of energy smaller than E_g are not absorbed by or emitted from the cell. We note that the transmissivity used in Eq. (1) includes contributions from all modes at the given frequency, and can in principle be larger than one.

When taking $\Delta\mu = 0$, $\dot{N}(T_{cell}, 0; T_s)$ represents the maximum current available for the load current for a given temperature difference. In this case, however, the generated e-h flux cannot maintain any non-zero voltage across the external load, leading to a zero output power. In reality, a non-zero $\Delta\mu$ is developed (when the external load is connected to the PV/TR cell) to maintain a non-zero output power. Depending on the load resistance, there exists an optimal $\Delta\mu$ for the maximum efficiency and a $\Delta\mu_{MP}$ for the maximum output power. From Eq. (1), the net photon current and the power for given T_{cell} and T_s are given by

$$\begin{aligned} I(\Delta\mu) &= e\dot{N}(T_{cell}, \Delta\mu; T_s), \\ P_{load}(\Delta\mu) &= \frac{\Delta\mu}{e} \cdot I(\Delta\mu) = \Delta\mu \cdot \dot{N}(T_{cell}, \Delta\mu; T_s) \end{aligned} \tag{2}$$

The net radiative power absorbed by the cell is given by

$$P_c(T_{cell}, \Delta\mu; T_s) = \int_0^{\infty} \frac{d\omega}{2\pi} \hbar\omega \cdot \varepsilon_{c,s}(\omega) \left[\Theta(\omega; T_s, 0) - \Theta(\omega; T_{cell}, \Delta\mu)\right]. \tag{3}$$

In PV devices, $P_c > 0$, meaning the PV cell obtains energy from the thermal reservoir (heat source). In TR device, $P_c < 0$, meaning TR cell gives energy to the thermal reservoir (heat sink). In the following discussions, the lower bound of the integral is replaced by ω_g, under the assumption that photons of below-gap energies are not absorbed. This assumption overestimates the efficiency, but does not change the output power. For TR devices, the efficiency is defined as [1]

$$\eta_{TR} = \frac{P_{load}(\Delta\mu)}{\dot{Q}_{in}} = \frac{P_{load}(\Delta\mu)}{P_{load}(\Delta\mu) + \dot{E}_{rad} - \dot{E}_{abs}} = \frac{P_{load}(\Delta\mu)}{P_{load}(\Delta\mu) - P_c(T_{cell}, \Delta\mu; T_s)} \tag{4}$$

Here, $\dot{E}_{rad}$ and $\dot{E}_{abs}$ are respectively the energy flux radiated from and absorbed by the cell, and $\dot{E}_{rad} - \dot{E}_{abs}$ is the net emission power from the TR cell. Note $P_c < 0$ for TR devices, ensuring $\eta_{TR} < 1$. With the formalism, the transmissivity is the most crucial quantity to compute or to approximate, and it generally depends on materials (through the dielectric functions) and geometry. While the formalism presented above is equivalent to that used in Ref. [4], it avoids the complications from entropic contribution (which is taken into account by the generalized Planck distribution) and thus allows a convenient comparison between the PV and TR devices. We now analyze TR performance for some cases in which the transmissivity can be expressed analytically.

B. Blackbody heat sink for TR devices

For the blackbody of flat surface, the transmissivity is given by [30]

$$\varepsilon_{c,s}(\omega) = 2 \times \frac{1}{(2\pi)^2} \int \varepsilon_{c,s}(\omega, \mathbf{K}) d^2\mathbf{K} = \frac{2}{2\pi} \int_0^{\omega/c} k dk = \frac{1}{2\pi} (\frac{\omega}{c})^2 \tag{5}$$

Note that the transmissivity is dimensionless by definition, and Eq. (5) has a dimension of $1/L^2$ (L stands for the length) as it is the transmissivity per unit area. $\mathbf{K}$ is the in-plane momentum and $|\mathbf{K}| = k$. In Eq. (5), we have used the momentum-dependent transmissivity: $\varepsilon_{c,s}(\omega, k)$ is one inside the light-cone $k < \omega/c$, and zero outside the light cone [30]. Using Eq. (5), the TR output power can be computed using the equations given in the previous subsection, and the results are identical to those given in Ref. [1]. As the blackbody surfaces is the upper limit of radiative transfer in the far-field based devices, we use it as the reference for comparison.

For the near-field device where the radiative energy transfer is governed by resonances, the momentum-dependent $\varepsilon_{c,s}(\omega, \mathbf{K})$ has a very weak $\mathbf{K}$ dependence when ω is around the resonant frequency ω_0. Consequently, the momentum integrated transmissivity $\varepsilon_{c,s}(\omega)$ becomes much larger than unity when $\omega \sim \omega_0$, which, from CMT point of view, is the origin of the near-field enhancement [30]. We shall establish that the δ-function transmissivity is a good approximation in this case.

C. δ-function transmissivity for TR devices

In this subsection we consider the δ-function transmissivity [3],

$$\varepsilon_{s,c}(\hbar\omega) = A\delta(\hbar\omega - \hbar\omega_0), \tag{6}$$

with $\omega_0 > \omega_g$ and A a constant. ω_0 is referred to as the resonant frequency. As $\varepsilon_{s,c}$ has the dimension of inverse of an area, A has the dimension of energy divided by the area. Due to its simplicity and relevancy to the later discussion, we provide more details. We will show that Eq. (6) is a good approximation when resonant modes are responsible for the radiative energy transfer, which is typical in the near-field devices [20, 30] (see Section III). One notes that A in Eq. (6) is geometry and material dependent. For example, the smaller vacuum gap between heat sink and TR cell gives a larger A. More generally, A is large when the TR cell and the heat sink satisfy the "impedance-matching" condition. The load output power is given by

$$P_{load}(\Delta\mu, \omega_0; T_s, T_{cell}) = A\frac{\Delta\mu}{2\pi}\left[\Theta(\omega_0; T_s, 0) - \Theta(\omega_0; T_{cell}, \Delta\mu)\right]. \tag{7}$$

The net radiative power absorbed by the cell is given by

$$P_c(T_{cell}, \Delta\mu; T_s) = A\frac{\hbar\omega_0}{2\pi}\left[\Theta(\omega_0; T_s, 0) - \Theta(\omega_0; T_{cell}, \Delta\mu)\right]. \tag{8}$$

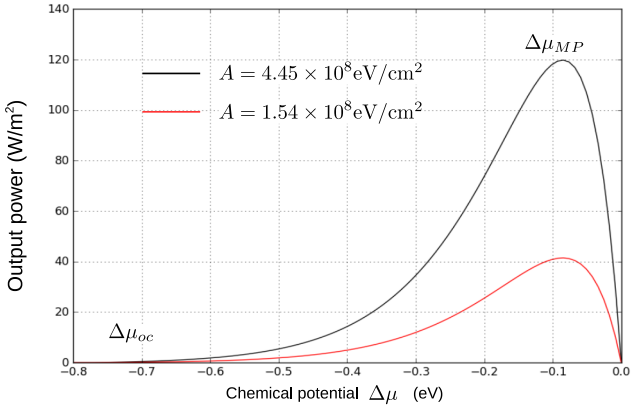

FIG. 2: Output power per unit area as a function of chemical potential, for δ-function transmissivity with amplitudes 4.45×10^8 eV/cm^2 (black curve) and 1.54×10^8 eV/cm^2 (red curve). They are δ-function approximations for the black and red curves in Fig. 3(c).

For TR devices, $\Delta\mu < 0$, the efficiency is given by

$$\eta_{TR} = \frac{\Delta\mu}{\Delta\mu - \hbar\omega_0} = \frac{|\Delta\mu|}{|\Delta\mu| + \hbar\omega_0} = \frac{|\Delta\mu|/(\hbar\omega_0)}{1 + |\Delta\mu|/(\hbar\omega_0)} \tag{9}$$

The open circuit $\Delta\mu_{oc}$ is given by the zero current, i.e. $\Theta(\omega_0;T_s,0)-\Theta(\omega_0;T_{cell},\Delta\mu_{oc})=0$, which is the largest possible value of $|\Delta\mu|$. This condition gives $\left[e^{\hbar\omega_0/T_s}-1\right]^{-1}=\left[e^{(\hbar\omega_0-\Delta\mu_{oc})/T_{cell}}-1\right]^{-1}$ and thus $1+\frac{|\Delta\mu_{oc}|}{\hbar\omega_0}=\frac{T_{cell}}{T_s}$. Substituting this expression into Eq. (9), we have $\eta_{TR}=1-\frac{T_s}{T_{cell}}$, which is the Carnot efficiency. The analysis shows that for δ-function transmissivity of any resonant frequency ω_0, the maximum efficiency is the Carnot efficiency at open-circuit voltage. Note that at this condition, the load output power is zero. For this reason we choose the maximum output power to gauge the TR performance.

Eq. (7) gives the load output power as a function of $\Delta\mu$. Two features are worth noting. First, Eq. (7) implies that larger value of A leads to a greater output power. This means that using the resonant modes and impedance-matching principle can greatly enhance the output power (see Section III). Second, we can numerically find the chemical potential $\Delta\mu_{MP}$ corresponding to the maximum output power, which is typically 10 to 20 % of the $\Delta\mu_{oc}$. This is in contrast to the PV devices, where $\Delta\mu_{MP}\lesssim\Delta\mu_{oc}$. Fig. 2 gives the example for $\hbar\omega_0=0.33$ eV, $\Delta\mu_{oc}=\hbar\omega_0\times(1-T_{cell}/T_s)=-0.77$ eV, and $A=4.45\times10^8$ eV/cm^2 and 1.54×10^8 eV/cm^2; these values correspond the near-field configurations which we shall discuss in Section III.

To conclude this subsection, we emphasize the following properties specific to the δ-function transmissivity for TR devices. Once $\hbar\omega_0>E_g$, the bandgap E_g does not affect the photon current and thus load output power, but a smaller $\hbar\omega_0$ gives a higher efficiency η_{TR} for the same $\Delta\mu$. The Carnot efficiency can be reached at the open-circuit chemical potential $\Delta\mu_{oc}$ for all resonant energies $\hbar\omega_0$, whose amplitude $|\Delta\mu_{oc}|$ can easily exceed the bandgap and resonant energy. However, at $\Delta\mu_{oc}$ the load output power is zero. Finally, $\Delta\mu_{MP}$ (~-0.08 eV) is generally 10 - 20 % of $\Delta\mu_{oc}$ (~-0.77 eV) in amplitude. The load output power is the quantity of interest for applications, and the way to enhance it is to increase the transmissivity.

III. NEAR-FIELD THERMORADIATIVE DEVICES

A. Configuration and material parametrization

We now consider some practical configurations for near-field TR devices – a TR cell at high temperature T_h and a heat sink at low temperature T_l, separated by a vacuum gap of width d [Fig. 3(a)]. The TR cell, just like a PV cell, is a semiconductor used to generate electric current. In the following discussion, we use $d=10$ nm, and only consider the radiative processes [1, 5]. For the TR cell, the dielectric function is governed by the direct valence-to-conduction interband transition [44, 45].

$$\begin{aligned}\epsilon_{pv}(\omega)&=\epsilon_r(\omega)+i\epsilon_i(\omega)\\ \epsilon_i(\omega)&=\begin{cases}A\sqrt{x-1}/x^2, & x>1\\ 0, & x<1\end{cases}\\ \epsilon_r(\omega)&=\begin{cases}B+A(2-\sqrt{1+x})/x^2, & x>1\\ B+A(2-\sqrt{1+x}-\sqrt{1-x})/x^2, & x<1\end{cases}.\end{aligned}\tag{10}$$

with $x=\hbar\omega/E_g$. As a model calculation, we use $(A,B,E_g)=(6,\,10,\,0.3\text{ eV})$ [39]. Here, 0.3 eV roughly corresponds to the bandgap of InAs [46] and bulk Black Phosphorous [47, 48]. We have varied A and B between 1 and 15, which are the typical values extracted from Refs. [44, 45], and found these values do not change the general behavior.

Three types of heat sink designs are considered: the metal heat sink, the Lorentz heat sink, and the heat sink which is the same as the TR cell, with the blackbody heat sink as the reference. Both metal and Lorentz material support the surface plasmon polariton mode. In the static limit, the surface resonant frequency ω_0 is given by $\epsilon(\omega_0)=-1$. Based on the impedance matching condition [32], when the surface mode and E_g are close in energy (with the former slightly larger), one gets a large transmissivity. We use $\hbar\omega_0=1.1\cdot E_g$. For the first design, the dielectric function of a metal can be approximated by the Drude model:

$$\epsilon_m=1-\frac{\omega_p^2}{\omega^2+i\gamma_m\omega}.\tag{11}$$

The surface resonant frequency is given by $\omega_0=\omega_p/\sqrt{2}$, so we choose $\omega_p=\sqrt{2}\times1.1\cdot E_g/\hbar$, and the decay rate is chosen to be $\gamma_m=0.002\omega_p$ (corresponding to Ag). We note that this decay rate is relatively small, and will show

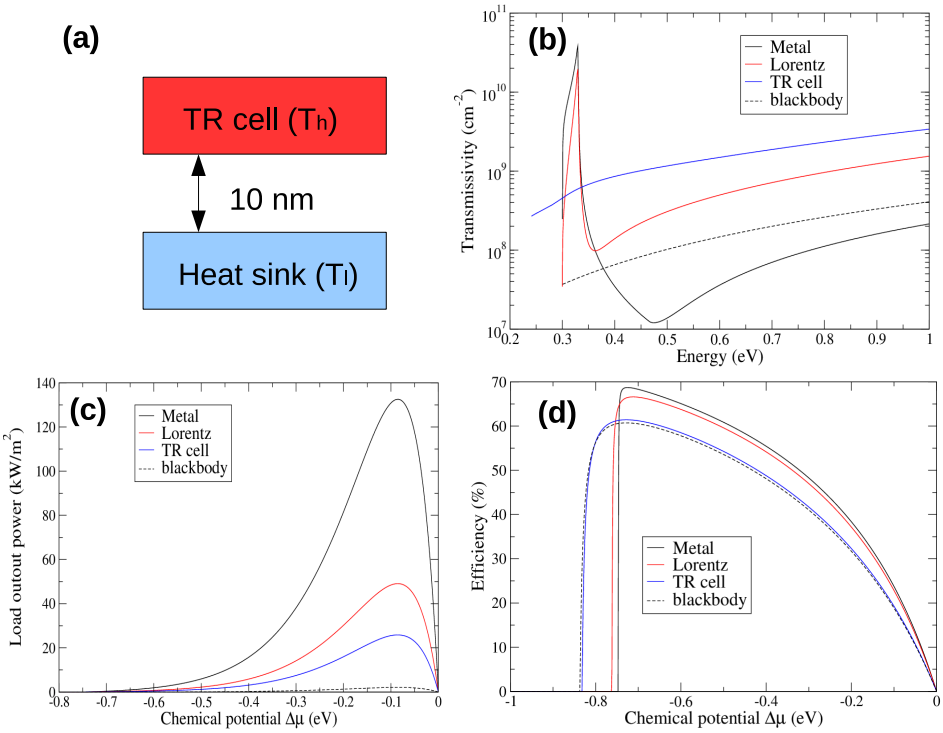

FIG. 3: (a) The simple near-field TR device. The TR cell, a semiconductor used as a current source, is at $T_h = 1000$ K. A heat sink is placed below the TR cell at a low temperature $T_l = 300$ K, with small vacuum gap (10 nm). (b) The transmissivity, (c) the load output power per unit area, and (d) the TR efficiency for metal, Lorentz, TR cell sinks. The blackbody assumes the TR cell is a blackbody for all energies above the bandgap. The Carnot efficiency is 70 % for the given temperatures. The δ-function approximations of (c) are given in Fig. 2, where about 90 % of load output power spectra for metal and Lorentz heat sinks are captured.

in the next subsection that increasing the decay rate (such as Pt with $\gamma_m \sim 0.013\omega_p$ or Al with $\gamma_m \sim 0.011\omega_p$) can increase the TR output power. The typical plasma frequency is of the order of eV, but introducing the nano-grating structure can create the geometry-induced resonances of much lower resonant frequencies [49, 50]. For the second design, the Lorentz material means its dielectric function can be described by the Lorentz oscillator model as

$$\epsilon_L(\omega) = \epsilon_\infty \frac{\omega^2 - \omega_{LO}^2 + i\gamma\omega}{\omega^2 - \omega_{TO}^2 + i\gamma\omega}. \tag{12}$$

This is typical for many insulators. Here we choose $\epsilon_\infty = 4.46$, $\omega_{TO}/\omega_{LO} = 0.81$, and $\gamma/\omega_{LO} = 0.0041$. The resonant frequency is given by $\omega_0^2 = \frac{\omega_{LO}^2 + \omega_{TO}^2/\epsilon_\infty}{1+1/\epsilon_\infty}$, which is set to $(1.1 \cdot E_g/\hbar)^2$. The parameter choice is motivated by cBN (cubic Boron Nitride) [20], with an enlarged longitudinal optical (LO) phonon frequency ω_{LO}. The third design of using the same materials for TR cell and heat sink is inspired by its symmetric configuration, which is shown to greatly enhance the transmissivity for both metal and Lorentz materials [20, 30, 32]. We shall assume the dielectric function is temperature independent over the temperature range of interest, and consequently the transimissivity is also temperature independent.

B. Results and discussions

Fig. 3 shows our calculated results for $T_{cell} = T_h = 1000$ K, $T_s = T_l = 300$ K. Fig. 3(b) gives the transmissivity between the TR cell and various heat sinks. For the metal and Lorentz heat sinks, there is a strong peak around their surface resonant energy (chosen to be around $1.1 \cdot E_g = 0.33$ eV for $E_g = 0.3$ eV), whose amplitude is a few hundred times larger than that of the blackbody reference. The corresponding maximum load output powers, shown

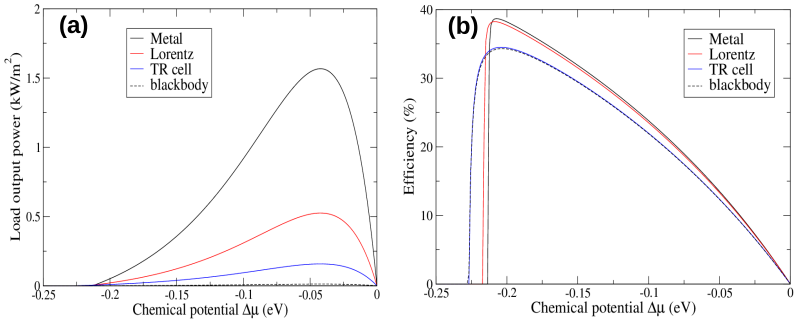

FIG. 4: (a) the load output power per unit area and (b) the TR efficiency for metal, Lorentz, TR-cell and blackbody heat sinks. The TR cell is at $T_h = 500$ K. A heat sink with small vacuum gap (10 nm) is placed below the TR cell with a low temperature $T_l = 300$ K. The Carnot efficiency is 40 % for the given temperatures.

in Fig. 3(c), are about 62 times (metal heat sink) and 23 times (Lorentz heat sink) greater than the blackbody reference. Since a strong peak in transmissivity can be approximated by a δ-function, we notice that the maximum efficiency, shown in Fig. 3(d), is very close to the Carnot efficiency (70 % in this case) at open-circuit $\Delta\mu$. To make the δ-function approximation more quantitative, we fix the coefficient A in Eq. (6) by integrating the black (metal) and red (Lorentz) curves in Fig. 3(b) between 0.3 eV and 0.4 eV, and the resulting load output power per area as a function of chemical potential are given in Fig. 2. Compared Fig. 2 with the exact solutions in Fig. 3(c), the δ-function transmissivity captures up to 90% of the total output power for both metal and Lorentz heat sinks, and can be regarded as the idealized model of the near-field transmissivity.

For the TR-cell heat sink, there is no peak structure in transmissivity, but the symmetric configuration makes its value about 10 times larger than the blackbody reference. The resulting maximum load output power is 12 times larger than the blackbody reference. As keeping TR cell at 1000 K may be too high in practice, we repeat the same analysis by using $T_{cell} = T_h = 500$ K. The load output power and efficiency are given in Fig. 4. The output powers are reduced in values, but the same enhancement is clearly observed. The same trend happens for the same T_h and T_l with a semiconductor of a larger bandgap (not shown) [50].

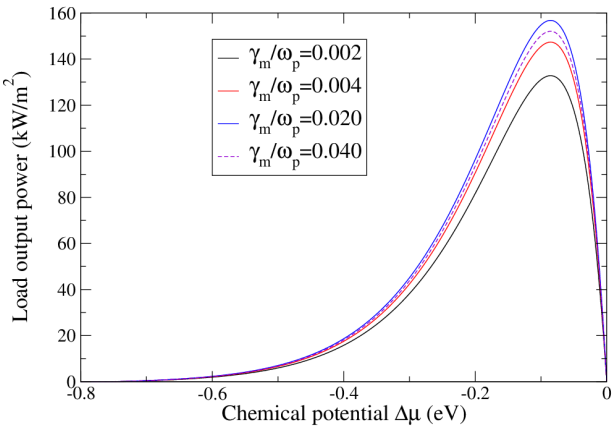

FIG. 5: The load output power per unit area for metal heat sink at $T_l = 300$ K. The TR cell is at $T_h = 1000$ K. Different decay rates of metal are compared. According to CMT, there exists an optimal decay rate, which in this configuration is about $\gamma_e/\omega_p = 0.02$, above and below which the output power decreases.

We now discuss our results from the point of CMT. In our simulations, the metal and Lorentz heat sinks are better than the TR-cell heat sink. This stems from the fact that the metal/vacuum and Lorentz/vacuum interfaces both support the surface plasmon polariton mode. Mathematically, the existence of surface mode means that $\epsilon(\omega_0) = -1$ has real-value solutions of ω_0, and this condition implies all modes of different in-plane momentum $\mathbf{K}$ have similar

resonant energy [51]. When the TR cell and the heat sink are spatially close, modes from a wide range of $\mathbf{K}$ can contribute to the transmissivity over a small energy window centered at $\hbar\omega_0$, leading to a strongly peaked, δ-function like transmissivity. This is in contrast to the far-field consideration, where the mode of large $|\mathbf{K}|$ corresponds to a large ω, leading to a smoother transmissivity of ω^2 dependence.

Our results show that the metal heat sink is more efficient than the Lorentz heat sink. According to CMT, this originates from the impedance-matching condition regarding to the decaying rate, i.e. the difference of resonance decaying rates to the metal and to the TR cell is *smaller* that that to the Lorentz material and to the TR cell. Moreover, CMT shows that there exists an optimal decay rate for the maximum transmissivity and thus the maximum load output power. We use the metal heat sink as the example, and the same behavior is found for the Lorentz heat sink. As shown in Fig. 5, when increasing the decay rate γ_e [defined in Eq. (11)], the output power first increases and then decreases. For this configuration, the optimal decaying rate is around $\gamma_e/\omega_p = 0.02$, above and below which the output power is smaller. From this analysis, the damping can sometimes be *beneficial* to the near-field TR devices, which is also the case for the near-field TPV [19]. As metals generally have large thermal conductivities than insulators, they are easier to dissipate heat and thus easier to be maintained at the ambient (low) temperature, which is another advantage for using metal as the heat sink. Generally the plasma frequency is high, we expect by grating the metal sink, which creates some geometry-dependent resonant modes [49, 50] can further enhance the output power, especially for the TR cell working at a lower temperature.

It is also worth noting that, although there is no surface resonance supported by the TR cell/vacuum interface, using TR cell as the heat sink automatically satisfies impedance-matching condition (the decaying rates to the TR cell and to the TR-cell heat sink are identical), and still significantly enhances the TR performance (10 times larger than the blackbody reference). This enhancement can also be understood from the enhanced photon density of states due to the refractive index ($n^2 \approx \epsilon$, with n the refractive index) [52–54]. The factor of ten enhancement is consistent with the model parameter we choose. As the maximum photon flux is limited by the largest refractive index of the TR cell and the heat sink, when no resonant modes are present, the symmetric configuration is the configuration of maximum photon flux for a chosen TR cell. Finally we comment on other non-radiative e-h processes, notably the impurity and Auger processes, neglected in the current ideal treatment. Inclusion of these processes reduces the load output power, and is important for applications. However, as these processes occur for both reference and designed configurations, we expect the enhancement *ratio* between the near-field heat sink and the blackbody reference to be approximately unchanged.

IV. CONCLUSION

In this work, we show that the load output power and efficiency for both PV and TR devices can be formulated using the generalized Planck distribution and the transmissivity. In this framework, the transmissivity is the most fundamental quantity to compute or model, and determines the performance of both PV and TR devices. For the ideal far-field device (blackbody limit), the transmissivity is known to have ω^2 frequency dependence; we establish that the δ-function transmissivity is a good approximation for the near-field devices whose radiative energy transfer is dominated by resonances. For the TR devices, the close-to Carnot efficiency can be achieved at the open-circuit chemical potential with a zero load output power, therefore we use the maximum load output power to gauge the TR performance. We compute the TR load output power using metal (Drude model), Lorentz (Lorentz oscillator model), and the same TR-cell material as the near-field heat sink. We find that, by choosing the energy of the surface plasmon polariton close to the bandgap of the TR cell, the metal and Lorentz heat sinks can enhance the output power by about 60 and 20 times respectively, as compared to the blackbody reference. The strong enhancement originates from the surface plasmon polariton supported by the heat sink/vacuum interface. Even for the TR-cell heat sink that does not support surface modes, the output power is still about 10 times larger. A general way to increase the transmissivity is to introduce more resonance modes. In view of this, we expect by grating the heat sink, which creates some geometry-specific resonant modes, by decorating heat sink with nanoparticles, or by adding interfaces

at the TR-cell side, can further enhance the TR performance.

---

[1] R. Strandberg, Journal of Applied Physics **117**, 055105 (2015), http://dx.doi.org/10.1063/1.4907392, URL http://dx.doi.org/10.1063/1.4907392.

[2] R. Strandberg, Journal of Applied Physics **118**, 215102 (2015), http://dx.doi.org/10.1063/1.4936614, URL http://dx.doi.org/10.1063/1.4936614.

[3] P. Santhanam and S. Fan, Phys. Rev. B **93**, 161410 (2016), URL http://link.aps.org/doi/10.1103/PhysRevB.93.161410.

[4] W.-C. Hsu, J. K. Tong, B. Liao, Y. Huang, S. V. Boriskina, and G. Chen, Scientific Reports **6**, 34837 (2016/10/13/online), URL http://dx.doi.org/10.1038/srep34837.

[5] W. Shockley and H. J. Queisser, Journal of Applied Physics **32**, 510 (1961).

[6] P. Würfel, *Physics of Solar Cells* (Wiley-vch, 2005).

[7] P. A. Davies and A. Luque, Solar Energy Materials and Solar Cells **33**, 11 (1994), ISSN 0927-0248, URL http://www.sciencedirect.com/science/article/pii/0927024894902844.

[8] N.-P. Harder and P. Würfel, Semiconductor Science and Technology **18**, S151 (2003), URL http://stacks.iop.org/0268-1242/18/i=5/a=303.

[9] P. Bermel, M. Ghebrebrhan, W. Chan, Y. X. Yeng, M. Araghchini, R. Hamam, C. H. Marton, K. F. Jensen, M. Soljačić, J. D. Joannopoulos, et al., Opt. Express **18**, A314 (2010), URL http://www.opticsexpress.org/abstract.cfm?URI=oe-18-103-A314.

[10] Y. X. Yeng, W. R. Chan, V. Rinnerbauer, J. D. Joannopoulos, M. Soljačić, and I. Celanovic, Opt. Express **21**, A1035 (2013), URL http://www.opticsexpress.org/abstract.cfm?URI=oe-21-106-A1035.

[11] A. Lenert, D. M. Bierman, Y. Nam, W. R. Chan, I. Celanović, M. Soljacic, and E. N. Wang, Nat Nano **9**, 126 (2014), URL http://dx.doi.org/10.1038/nnano.2013.286.

[12] D. M. Bierman, A. Lenert, W. R. Chan, B. Bhatia, I. Celanović, M. Soljacic, and E. N. Wang, Nature Energy **1**, 16068 (2016), URL http://dx.doi.org/10.1038/nenergy.2016.68.

[13] M. Laroche, R. Carminati, and J.-J. Greffet, Journal of Applied Physics **100**, 063704 (2006), URL http://dx.doi.org/10.1063/1.2234560.

[14] S. Basu, Y.-B. Chen, and Z. M. Zhang, International Journal of Energy Research **31**, 689 (2007), ISSN 1099-114X, URL http://dx.doi.org/10.1002/er.1286.

[15] M. Francoeur, R. Vaillon, and M. P. Meng, IEEE Transactions on Energy Conversion **26**, 686 (2011), ISSN 0885-8969.

[16] O. Ilic, M. Jablan, J. D. Joannopoulos, I. Celanovic, and M. Soljačić, Opt. Express **20**, A366 (2012), URL http://www.opticsexpress.org/abstract.cfm?URI=oe-20-103-A366.

[17] R. Messina and P. Ben-Abdallah, Scientific Reports **3**, 1383 (2013), URL http://dx.doi.org/10.1038/srep01383.

[18] T. J. Bright, L. P. Wang, and Z. M. Zhang, Journal of Heat Transfer **136**, 062701 (2014).

[19] A. Karalis and J. D. Joannopoulos, Scientific Reports **6**, 141108 (2016), URL http://dx.doi.org/10.1038/srep28472.

[20] A. Narayanaswamy and G. Chen, Applied Physics Letters **82**, 3544 (2003), URL http://scitation.aip.org/content/aip/journal/apl/82/20/10.1063/1.1575936.

[21] C. Fu and Z. Zhang, International Journal of Heat and Mass Transfer **49**, 1703 (2006), ISSN 0017-9310, URL http://www.sciencedirect.com/science/article/pii/S0017931005006502.

[22] X. Liu, L. Wang, and Z. M. Zhang, Nanoscale and Microscale Thermophysical Engineering **19**, 98 (2015), URL http://dx.doi.org/10.1080/15567265.2015.1027836.

[23] B. Song, A. Fiorino, E. Meyhofer, and P. Reddy, AIP Advances **5**, 053503 (2015), URL http://dx.doi.org/10.1063/1.4919048.

[24] H. A. Haus and W. Huang, Proceedings of the IEEE **79**, 1505 (1991), ISSN 0018-9219.

[25] A. W. Snyder, J. Opt. Soc. Am. **62**, 1267 (1972), URL http://www.osapublishing.org/abstract.cfm?URI=josa-62-11-1267.

[26] W.-P. Huang, J. Opt. Soc. Am. A **11**, 963 (1994), URL http://josaa.osa.org/abstract.cfm?URI=josaa-11-3-963.

[27] S. Fan, W. Suh, and J. D. Joannopoulos, J. Opt. Soc. Am. A **20**, 569 (2003), URL http://josaa.osa.org/abstract.cfm?URI=josaa-20-3-569.

[28] L. Zhu, S. Sandhu, C. Otey, S. Fan, M. B. Sinclair, and T. Shan Luk, Applied Physics Letters **102**, 103104 (2013), URL http://scitation.aip.org/content/aip/journal/apl/102/10/10.1063/1.4794981.

[29] H. Chalabi, E. Hasman, and M. L. Brongersma, Opt. Express **22**, 30032 (2014), URL http://www.opticsexpress.org/abstract.cfm?URI=oe-22-24-30032.

[30] A. Karalis and J. D. Joannopoulos, Applied Physics Letters **107**, 141108 (2015), URL http://scitation.aip.org/content/aip/journal/apl/107/14/10.1063/1.4932520.

[31] C. Lin, B. Wang, and K. H. Teo, Journal of Applied Physics **121**, 183101 (2017), URL http://dx.doi.org/10.1063/1.4983021.

[32] C. Lin, B. Wang, K. H. Teo, and P. Bandaru, Phys. Rev. Applied **7**, 034003 (2017), URL https://link.aps.org/doi/10.1103/PhysRevApplied.7.034003.

[33] P. Würfel, Journal of Physics C: Solid State Physics **15**, 3967 (1982), URL http://stacks.iop.org/0022-3719/15/i=18/a=012.

[34] B. Feuerbacher and P. Würfel, Journal of Physics: Condensed Matter **2**, 3803 (1990), URL http://stacks.iop.org/0953-8984/2/i=16/a=010.

[35] P. Würfel, S. Finkbeiner, and E. Daub, Applied Physics A **60**, 67 (1995), ISSN 1432-0630, URL http://dx.doi.org/10.1007/BF01577615.

[36] E. N. Economou, Phys. Rev. **182**, 539 (1969), URL http://link.aps.org/doi/10.1103/PhysRev.182.539.

[37] E. N. Economou and K. L. Ngai, *Surface Plasma Oscillations and Related Surface Effects in Solids* (John Wiley & Sons, Inc., 2007), pp. 265–354, ISBN 9780470143797, URL http://dx.doi.org/10.1002/9780470143797.ch3.

[38] W. G. Spitzer, D. Kleinman, and D. Walsh, Phys. Rev. **113**, 127 (1959), URL http://link.aps.org/doi/10.1103/PhysRev.113.127.

[39] M. I. Eremets, M. Gauthier, A. Polian, J. C. Chervin, J. M. Besson, G. A. Dubitskii, and Y. Y. Semenova, Phys. Rev. B **52**, 8854 (1995), URL http://link.aps.org/doi/10.1103/PhysRevB.52.8854.

[40] D. Polder and M. Van Hove, Phys. Rev. B **4**, 3303 (1971), URL http://link.aps.org/doi/10.1103/PhysRevB.4.3303.

[41] K. Joulain, J.-P. Mulet, F. Marquier, R. Carminati, and J.-J. Greffet, Surface Science Reports **57**, 59 (2005), ISSN 0167-5729, URL http://www.sciencedirect.com/science/article/pii/S0167572905000105.

[42] H. B. Callen and T. A. Welton, Phys. Rev. **83**, 34 (1951), URL http://link.aps.org/doi/10.1103/PhysRev.83.34.

[43] Generally, the photon chemical potential is determined by the resistance of the external load.

[44] D. E. Aspnes and A. A. Studna, Phys. Rev. B **27**, 985 (1983), URL http://link.aps.org/doi/10.1103/PhysRevB.27.985.

[45] S. Adachi, Phys. Rev. B **35**, 7454 (1987), URL http://link.aps.org/doi/10.1103/PhysRevB.35.7454.

[46] S. Adachi, Journal of Applied Physics **66**, 6030 (1989), http://dx.doi.org/10.1063/1.343580, URL http://dx.doi.org/10.1063/1.343580.

[47] C. D. Zhang, J. C. Lian, W. Yi, Y. H. Jiang, L. W. Liu, H. Hu, W. D. Xiao, S. X. Du, L. L. Sun, and H. J. Gao, The Journal of Physical Chemistry C **113**, 18823 (2009), http://dx.doi.org/10.1021/jp907062n, URL http://dx.doi.org/10.1021/jp907062n.

[48] A. Castellanos-Gomez, The Journal of Physical Chemistry Letters **6**, 4280 (2015), pMID: 26600394, URL http://dx.doi.org/10.1021/acs.jpclett.5b01686.

[49] Y. Yang and L. Wang, Phys. Rev. Lett. **117**, 044301 (2016), URL http://link.aps.org/doi/10.1103/PhysRevLett.117.044301.

[50] B. Wang, C. Lin, K. H. Teo, and Z. Zhang, Journal of Quantitative Spectroscopy and Radiative Transfer **196**, 10 (2017), ISSN 0022-4073, URL http://www.sciencedirect.com/science/article/pii/S0022407317301140.

[51] The condition $\epsilon(\omega_0) = -1$ is obtained assuming the infinite speed of light ($c \to \infty$), which is a good approximation for large $\mathbf{K}$. When the retardation effect is taken into account, a small dispersion at small $\mathbf{K}$ emerges.

[52] R. S. DiMatteo, P. Greiff, S. L. Finberg, K. A. YoungWaithe, H. K. H. Choy, M. M. Masaki, and C. G. Fonstad, AIP Conference Proceedings **653** (2003).

[53] R. DiMatteo, P. Greiff, D. Seltzer, D. Meulenberg, E. Brown, E. Carlen, K. Kaiser, S. Finberg, H. Nguyen, J. Azarkevich, et al., AIP Conference Proceedings **738** (2004).

[54] Z. Yu, N. P. Sergeant, T. Skauli, G. Zhang, H. Wang, and S. Fan, Nature Communications **4**, 1730 (2013), URL http://dx.doi.org/10.1038/ncomms2765.